Modulated ultrasonic elliptical vibration cutting for ductile-regime texturing of brittle materials with 2-D combined resonant and non-resonant vibrations

Jianjian Wang [a,b,c], Wei-Hsin Liao [b], Ping Guo [a,*]

[a] Department of Mechanical Engineering, Northwestern University, Evanston, IL, USA
[b] Department of Mechanical and Automation Engineering, The Chinese University of Hong Kong, China
[c] Shun Hing Institute of Advanced Engineering, The Chinese University of Hong Kong, China

ABSTRACT

In this study, modulated ultrasonic elliptical vibration cutting (modulated UEVC) is proposed to generate micro-structured surfaces on brittle materials in ductile-regime. A novel tool is first developed to generate 2-D combined resonant and non-resonant vibrations in a single compact structure. The ultrasonic elliptical vibration is excited at the coupled resonant frequency of 20 kHz to enhance the ductile-to-brittle transition depth, while the simultaneously generated non-resonant modulation motion (up to 2 kHz) is used to adjust the tool center to generate surface structures dynamically. A theoretical model is established to analyze the instantaneous uncut chip thickness in modulated UEVC by considering a more general case of an inclined elliptical vibration trajectory. The analysis indicates that the orientation angle of 135° is optimal to achieve the maximal critical depth-of-cut in ductile-regime cutting. Experimental results are provided to demonstrate the process capability and to verify the proposed theoretical model. Micro dimple arrays have been successfully generated using the proposed modulated UEVC for a depth-of-cut up to 700 nm in ductile-regime, and an extended depth-of-cut up to 1 μm with minimal surface damage.

1. Introduction

Micro-structured brittle materials represented by silicon, glass, tungsten carbide, etc. have a broad prospect in advanced optical applications [1]. For example, silicon and glass components with regular surface structures can be used as micro-optics for function integration and minimization of advanced optical systems [2], while tungsten carbide molds with micro-structured surfaces can be used for the mass fabrication of polymer optics [3]. Up to now, in optics and optical mold manufacturing, ultra-precision cutting using single-point diamond tools is still dominant. However, the direct machining of brittle materials with crack-free and micro-structured surfaces using single-point diamond tools is still challenging [4].

Single point diamond turning is able to directly machine brittle materials in the ductile-regime due to its capability to remove materials with extremely small chip thickness [5]. By limiting the depth-of-cut (DOC) within a critical value, the brittle materials can be removed by plastic chip flow at a fine scale, termed as ductile-regime cutting [6]. Single point diamond turning has also shown some promising results in ductile-texturing of micro-structured brittle materials with the combi-

nation of fast/slow tool servo techniques [7]. It offers a great advantage in terms of nanometric surface finish, stringent form accuracy, high flexibility, as well as the elimination of remounting and further polishing operations [8]. However, due to the low fracture toughness of brittle materials, the DOC in diamond turning is limited to a small range (e.g., 58 nanometers for silicon [9]) to avoid brittle fracture induced surface cracks [10]. The strictly limited critical DOC significantly restricts the machining efficiency, flexibility and achievable aspect ratio of micro-structures [11].

To improve the critical cutting depth in ductile-regime machining, ultrasonic elliptical vibration cutting (UEVC) has been successfully applied in the ultra-precision diamond cutting of many brittle materials including silicon [9], glass [12] and tungsten carbide [13]. In UEVC, ultrasonic elliptical vibration is added to a diamond tool to form overlapping tool trajectories [14] as shown in Fig. 1. The instantaneous uncut chip thickness is thus significantly reduced to the path difference between two vibration cycles even with a large nominal DOC [15]. If the maximal uncut chip thickness within a vibration cycle is kept below the ductile-to-brittle transition distance, ductile-regime cutting is achieved for much enhanced nominal DOC compared with conventional diamond
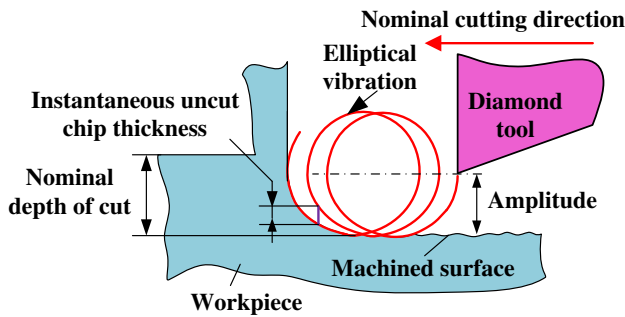

Fig. 1. Process principle of ultrasonic elliptical vibration cutting (UEVC) for brittle materials with reduced uncut chip thickness (to be more rigorously defined in Section 3).

cutting [16]. The improvement ratio of critical DOC has been reported up to 12.8 times for silicon [9]. Hence, UEVC is promising for ductile surface texturing of brittle materials with much-improved efficiency and capability [11].

In order to apply UEVC for ductile cutting of micro-structures on brittle surfaces, additional control of nominal depth-of-cut is essential for creating micro-structured surfaces. One solution is to dynamically adjust the elliptical vibration center by mounting the UEVC tool on a fast/slow tool servo [17]. However, this method is very limited in terms of fabrication efficiency due to the narrow working bandwidth of slow tool servo. Meanwhile, the UEVC tool is usually too heavy for a fast tool servo, which reduces its working bandwidth thus the fabrication efficiency significantly. Moreover, due to the strict conditions of ductile-regime cutting of brittle materials in terms of tool trajectories and positioning accuracy, no commercially available device could combine UEVC with a fast tool servo for ductile surface texturing of brittle materials [18, 19]. In order to overcome the problems mentioned above, an interesting strategy to use vibration amplitude control of UEVC for dynamic depth adjustment has been proposed to sculpture micro-structures on difficult-to-cut materials [20]. By controlling the vibration amplitude of UEVC in the DOC direction, micro-dimples and grooves have been successfully fabricated on tungsten carbide [21] and silicon [22]. The amplitude control method provides precise control of the cutting depth modulation, but is restricted by the low bandwidth of 300 Hz [20] and small feature depth (up to the vibration amplitude). Besides, the amplitude control method also changes effective uncut chip thickness, which might violate the ductile cutting condition if the vibration amplitude in the DOC direction is too small [9].

In addition, non-resonant vibration cutting has also been used for ductile machining of silicon. Wang et al. proposed a 2D high-bandwidth non-resonant tool to generate trapezoidal vibration to explore the possibility that non-harmonic vibration can further improve the critical ductile cutting depth of silicon compared with harmonic elliptical vibration [23]. Similar 2D non-resonant vibration tools have been developed by Zhou et al. [24] and Yuan et al. [25] to achieve dual-frequency elliptical vibration texturing. However, due to the limitation of natural frequency (<7 kHz [23], <2 kHz [24], <0.5 kHz [25]), these designs of non-resonant tool cannot generate ultrasonic elliptical vibration to texture micro-structures on silicon.

The current challenges to apply UEVC in ductile-regime texturing of micro-structured surfaces mainly lie in two aspects: (1) the minimum feature-length limited by the tool motion bandwidth and (2) the maximal feature depth limited by the critical ductile-to-brittle transition distance. In response to the above-stated challenges, we propose a modulated UEVC method to use 2-D combined resonant and non-resonant vibrations from a single tool to achieve high-bandwidth ductile texturing of brittle materials. We first present the design of a unique hybrid tool to operate in the resonant mode at 20 kHz for ultrasonic elliptical vibration cutting and simultaneously in the non-resonant mode within

2 kHz to provide cutting depth modulation. We further investigate the cutting mechanism and ductile-to-brittle transition in the proposed surface texturing process, especially the effect of orientation angle of ultrasonic elliptical trajectories on the critical cutting depth of a typical brittle material (single crystal silicon). We demonstrate the ductile texturing results of dimple arrays on silicon surfaces using the proposed method and compare the results with those obtained from conventional diamond cutting.

2. Modulated UEVC with 2-D combined resonant and non-resonant vibrations

The principle of modulated UEVC process using 2-D combined resonant and non-resonant vibrations is illustrated in Fig. 2. With a very compact tool structure, the 2-D vibration tool is designed to have its first two resonant modes in the ultrasonic range. The typical frequency response curve of the tool will resemble a second-order system as shown in Fig. 2. The output vibration amplitude is linearly related to the excitation voltage in the lower frequency range, while significantly amplified at the resonance in the ultrasonic frequency range. Owing to this unique frequency response characteristic, the 2-D vibration tool operates at the resonance frequency with very small excitation voltage to generate amplified elliptical vibration at a fixed ultrasonic frequency, while utilizing the flat frequency response in the lower frequency range to act as a non-resonant tool simultaneously. In this way, modulated ultrasonic elliptical vibration can be generated as shown in Fig. 2, where the ultrasonic elliptical vibration is utilized to increase the critical depth in ductile-regime cutting, while the non-resonant motion is used to dynamically modulate the elliptical vibration center to generate surface micro-structures. One unique innovation of this method is the utilization of the same structure and driving units to achieve combined vibration with a much wider operation bandwidth.

2.1. Tool design

The tool design is illustrated in Fig. 3(a), where the overall dimension is 36 mm × 36 mm × 10 mm. To generate combined resonant and non-resonant vibrations, the design of a 2-D vibration cutting tool utilizes a compact compliant structure actuated by two piezo stacks. The compact design sets the first two structural resonant modes in the ultrasonic frequency so that the lower frequency band will have a uniform response. The compliant structure, leaf-spring flexure hinge (LSFH), connects the piezo stack actuators (PSAs) and the end effector, which is used to transmit only the axial motion of piezo actuators and to decouple the cross-coupling. Based on the linear superposition principle, the resonant
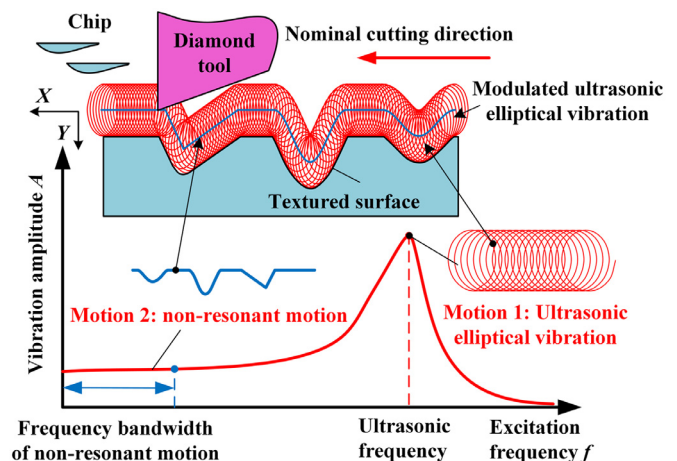

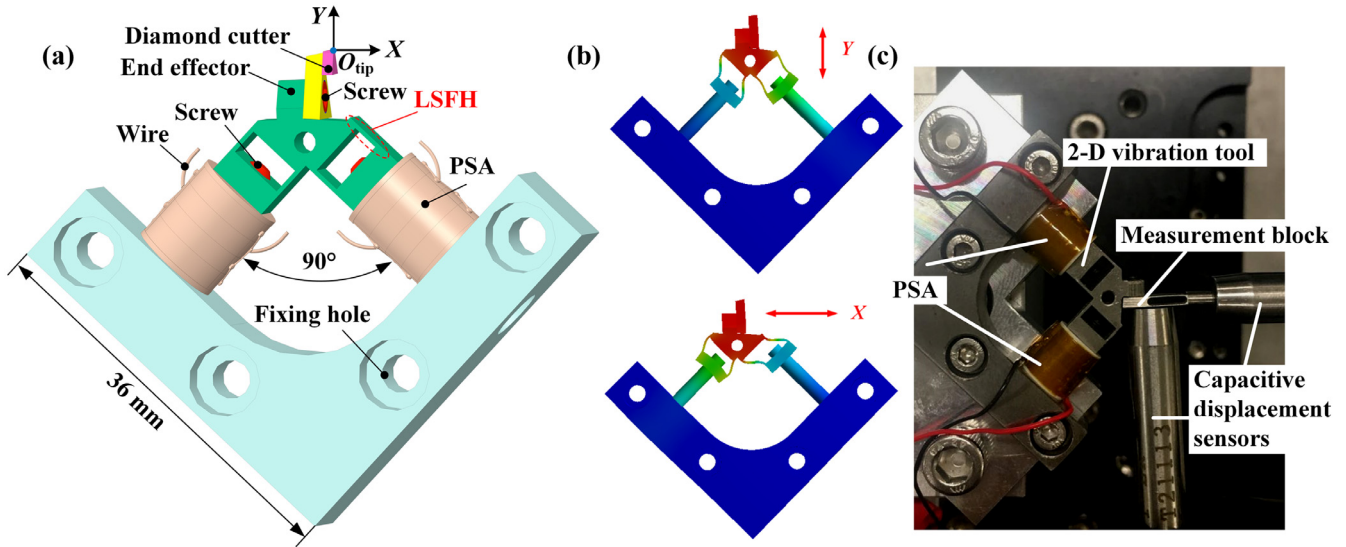**Fig. 2.** Modulated UEVC with a single 2-D vibration cutting tool.

Fig. 3. (a) Design of the proposed 2-D vibration tool; (b) modal analysis results of the first and second resonant modes in the *Y* (23.0 kHz) and *X* (23.4 kHz) directions; (c) measurement system of vibration amplitudes.

and non-resonant mode motions can be independently controlled without interfering with each other. The tool prototype was fabricated from spring steel for its high elasticity and fatigue strength. The end effector with the flexure hinges was machined from a single piece using wire electrical discharge machining.

A finite element method (FEM) model was set up using the actual tool dimensions and material properties for structural modal analysis. The simulation results are plotted in Fig. 3(b), where the first two resonant modes are identified at 23.0 kHz and 23. 4 kHz respectively. The vibration direction of the two modes is in accordance with the depth-of-cut (*Y*) and cutting (*X*) directions. Also, due to the deliberate design to have the two modes resonant at a similar frequency, mode coupling can be achieved to generate elliptical vibration in the cutting plane (*XY* plane) by adjusting the phase angles of the two-channel excitation signals [26]. The structure resonance can amplify the output amplitude from the PSAs up to five times at the ultrasonic resonant frequency, which is otherwise impossible to drive directly due to the extreme current requirement.

In the non-resonant mode, tool trajectories are determined by the geometrical configuration and direct output from the PSAs. As shown in Fig. 3(a), two orthogonally placed PSAs (model PK44K2P2, *Thorlabs*) are used to generate two independent motions, while two groups of parallel leaf-spring flexure hinges (LSFHs) are utilized for decoupling. Though in principle the non-resonant mode could have a bandwidth up to the first resonant frequency, its workspace and frequency bandwidth is limited by the current output of the piezo amplifier and heat generation from the dielectric loss, which is further analyzed in Section 2.3. Besides, the output stiffness at the tool tip was simulated to reach 14 N/μm in the cutting direction and 49 N/μm in the DOC direction, which would be adequate for the ductile-regime cutting at the nano-scale.

2.2. Evaluation of resonant mode operation

The ultrasonic elliptical vibration can be generated by exciting the PSAs at the coupled resonant frequency with an adjustable phase angle to tune the trajectory shape. The harmonic excitation signals can be described by:

$$\begin{bmatrix} U_{1L}(t) \\ U_{1R}(t) \end{bmatrix} = \begin{bmatrix} U_{1L,0-p} \sin\left(2\pi f_1 t\right) \\ U_{1R,0-p} \sin\left(2\pi f_1 t + \alpha_1\right) \end{bmatrix} \tag{1}$$

where U_{1L} and U_{1R} are the input voltages to the two PSAs; $U_{1L,0-p}$, $U_{1R,0-p}$, α_1, and f_1 are the amplitudes, phase angle, and frequency of the excitation signals.

According to Eq. (1), the frequency response curves were obtained by sine sweep tests in the cutting (*X*) and depth-of-cut (*Y*) directions using two capacitance displacement sensors and a measurement block (same mass as the cutting insert) as shown in Fig. 3(c). The results are shown in Fig. 4(a), where the pure *Y*-direction vibration was excited by setting $U_{1L,0-p} = U_{1R,0-p} = 3$ V and $\alpha_1 = 0°$; and the pure *X*-direction vibration was excited by setting $U_{1L,0-p} = U_{1R,0-p} = 3$ V and $\alpha_1 = 180°$ The excitation frequency was linearly swept from 0 to 25 kHz. The first two resonant frequencies can be identified from the measured results at 20.0 kHz and 22.0 kHz in the *Y*- and *X*-directions respectively. The discrepancy between simulation and experimental results of resonant frequencies can be attributed to (1) unconsidered contact stiffness of interfaces in the FEM simulation, including the interface between screw thread and end effector, and the interface between screw head and fixing block; (2) the manufacturing error of designed vibration tool, especially of manufacturing error of leaf-spring flexure hinge, which significantly affects the structural stiffness. When excitation frequency f_1 was fixed at 20 kHz, we measured the elliptical vibration trajectories for different phase angle $\alpha 1$ as shown in Fig. 4(b). The measured ultrasonic elliptical trajectories show the open-loop performance of the system, which can be further stabilized with a feedback control system.

2.3. Evaluation of non-resonant mode operation

The non-resonant motion can be generated by adjusting the input signals to the two PSAs subject to the geometric configuration as

$$\begin{bmatrix} u_{out}^x \\ u_{out}^y \end{bmatrix} = \begin{bmatrix} a_x & -a_x \\ a_y & a_y \end{bmatrix} \begin{bmatrix} U_{2L}(t) \\ U_{2R}(t) \end{bmatrix} \tag{2}$$

where u_{out}^x and u_{out}^y denote the output displacements at the tool tip along with the *X* and *Y* directions; a_x and a_y are the coefficients that relate the input voltage to the output displacement, which is calibrated as $a_x = 0.053$ μm/V and $a_y = 0.049$ μm/V. U_{2L} and U_{2R} are the input voltages to the two PSAs with amplitudes of $U_{2L,0-p}$, $U_{2R,0-p}$ and phase angle of α_2 respectively

The working space, coupling ratio, and trajectory controllability were experimentally evaluated for the non-resonant mode operation.
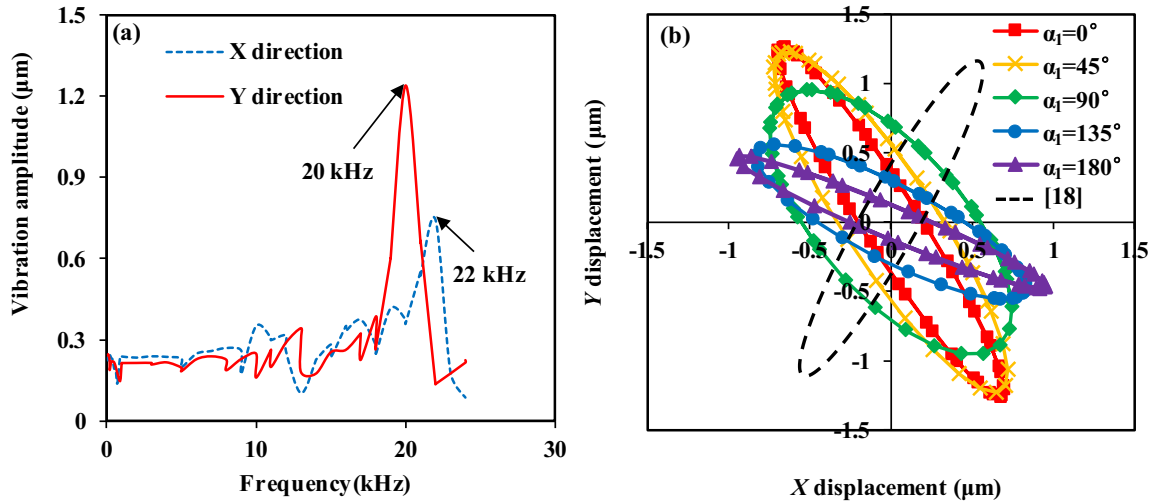
Fig. 4. (a) Experimental results of the dynamic tests: for X-direction, $U_{1L,\,0\text{-}p} = U_{1R,\,0\text{-}p} = 3$ V, $\alpha_1 = 180°$; for Y-direction, $U_{1L,\,0\text{-}p} = U_{1R,\,0\text{-}p} = 3$ V, $\alpha_1 = 0°$; (b) measured elliptical vibration trajectories for different phase angles ($f_1 = 20$ kHz, $U_{1L,0\text{-}p} = U_{1R,0\text{-}p} = 3$ V).
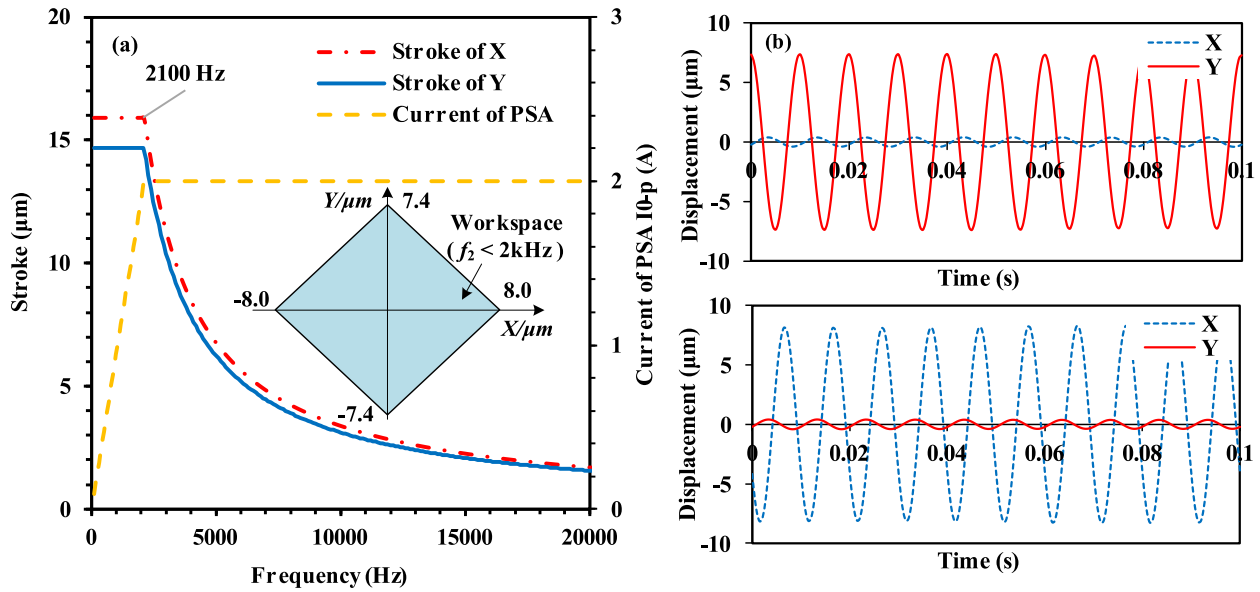

Fig. 5. (a) Dependency of motion strokes on the frequency; (b) results of coupling tests in the X- and Y-directions.

Firstly, the working space was obtained by considering the PSA stroke and the current needed to drive the PSA dynamically. The maximally achievable stroke is mainly constrained by the frequency-dependent characteristic of driving current, which can be estimated by the following relationship assuming a sinusoidal driving signal [27],

$$I_{0-p} = \pi \cdot f_2 \cdot C_{PSA} \cdot U_{p-p} \le I_m \qquad (3)$$

where $U_{p\text{-}p}$ is the peak-to-peak excitation voltage amplitude; C_{PSA} is the capacitance of the PSA; and f_2 is the driving frequency. The peak current $I_{0\text{-}p}$ is limited by the maximum current capacity I_m of the piezo voltage amplifier. In the current study, a voltage amplifier (PX200, *Piezo-Drive*) is used, which has a maximal current output of 2 A. The motion strokes of PSA are thus limited by its maximal stoke at low frequencies and limited by the current requirement at high frequencies according to Eq. (3). Fig. 5(a) shows the frequency dependency of working space, where the maximum working space of 16 μm × 15 μm can be achieved up to 2.1 kHz.

Secondly, the coupling tests were performed to evaluate the cross-coupling effect between the X- and Y-direction motions. Pure DOC vi-

bration (Y direction) was generated by setting $U_{2L,\,0\text{-}p} = U_{2R,\,0\text{-}p} = 75$ V with a phase angle α_2 of 0° The dominant direction and the parasite motions were both measured. The tests were repeated for the dominant motion in the cutting direction (X direction) by setting the phase angle α_2 to 180° The results are plotted in Fig. 5(b). Due to the adoption of two sets of leaf-spring flexure hinges, the cross-coupling ratios were measured to be less than 5%.

Finally, the controllability of the elliptical vibration trajectory at 100 Hz was evaluated with the results shown in Fig. 6. This non-resonant elliptical motion (with much precise control based on the geometric configuration) is utilized as a modulation motion to adjust the tool center position for the proposed modulated UEVC process.

2.4. Evaluation of combined resonant and non-resonant operation

The combined resonant and non-resonant vibrations can be generated by superimposing two sets of excitation signals. The first set is at the ultrasonic frequency to generate the resonant vibration, while the second set is within the non-resonant operation bandwidth to modulate
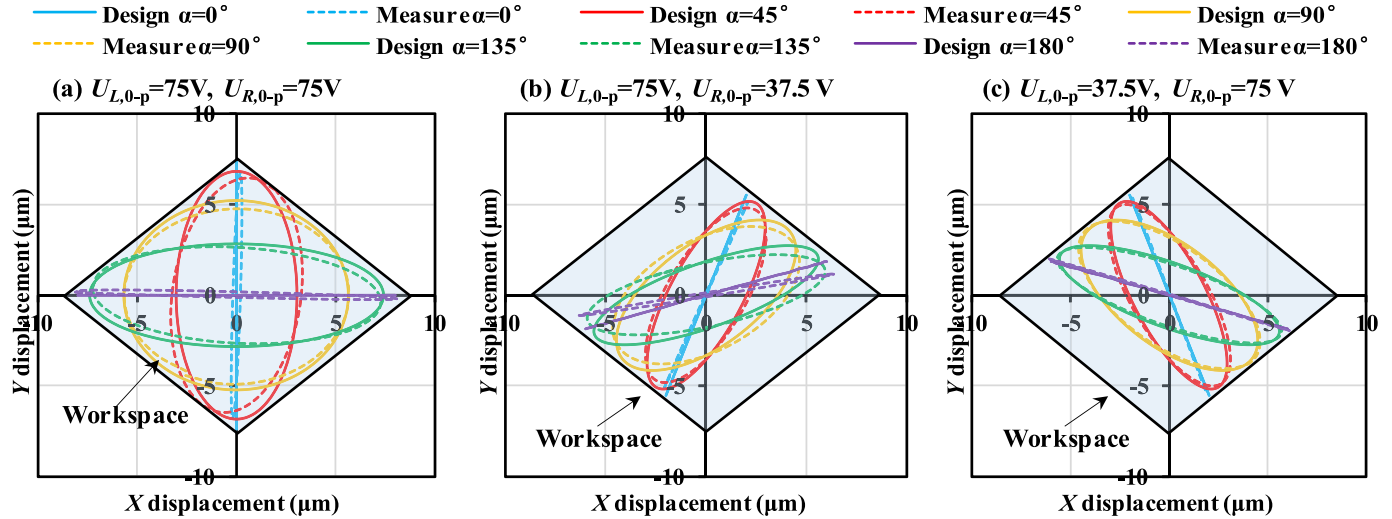
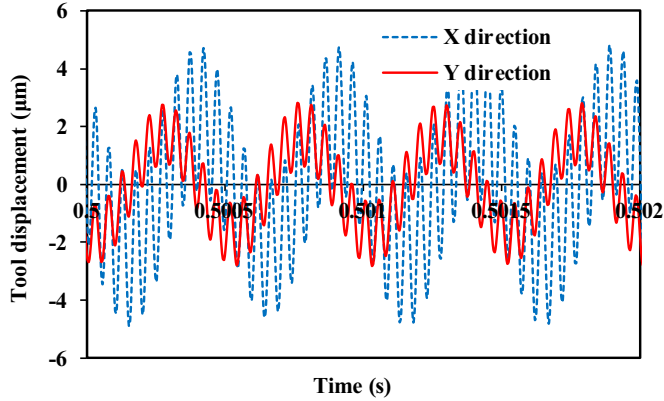Fig. 6. Comparison between designed and measured trajectories with different excitation conditions (f_2 = 100 Hz).

Fig. 7. Modulated motion due to the combined resonant and non-resonant vibrations (f_1 = 20 kHz and f_2 = 2 kHz, $U_{1L,0\text{-}p} = U_{1R,0\text{-}p}$ = 3 V, $U_{2L,0\text{-}p} = U_{2R,0\text{-}p}$ = 30 V, $\alpha_1 = \alpha_2 = 90°$).

the tool tip position. The combined excitation signals can be described by

$$\begin{cases} U_L(t) = U_{1L,0-p} \sin(2\pi f_1 t) + U_{2L,0-p} \sin(2\pi f_2 t) \\ U_R(t) = U_{1R,0-p} \sin(2\pi f_1 t + \alpha_1) + U_{2R,0-p} \sin(2\pi f_2 t + \alpha_2) \end{cases} \quad (4)$$

Again, f_1 and f_2 denote the high (usually ultrasonic) and low frequencies respectively; $U_{1L,0\text{-}p}$, $U_{1R,0\text{-}p}$, $U_{2L,0\text{-}p}$ and $U_{2R,0\text{-}p}$ are the corresponding signal amplitudes; α_1 and α_2 are the phase angles between the two-channel driving signals. As shown in Eq. (4), each PSA is actuated with excitation signals of both low and ultrasonic frequencies simultaneously. According to Eq. (4), the combined resonant and non-resonant vibration was experimentally verified with a typical case of measured vibration trajectories shown in Fig. 7. The detailed parameter settings are listed in the caption. The combined vibration was measured at 20 kHz and 2 kHz. As shown in Fig. 7, in the X direction, the non-resonant vibration signal with an amplitude of 2.5 μm and a frequency of 2 kHz is added to the resonant ultrasonic vibration with an amplitude of 2.5 μm. Meanwhile, in the Y direction, the non-resonant vibration signal with an amplitude of 1.8 μm and a frequency of 2 kHz is added to the resonant ultrasonic vibration with an amplitude of 1 μm. Due to the combined resonant and non-resonant vibrations, the ultrasonic frequency vibration center of each direction is modulated by the non-resonant motion of 2 kHz.

3. Analysis of cutting mechanism in modulated UEVC

Understanding of the ductile-to-brittle transition mechanism in modulated UEVC is the fundamental step to the determination of process parameters in ductile texturing of brittle materials. A theoretical model is established in this section to analyze the instantaneous uncut chip thickness and its maximum value in one vibration cycle in modulated UEVC, which plays a critical role in determining the critical cutting depth in ductile-regime machining [28, 29]. The proposed model extends the current understanding of UEVC [16] by considering a more general case of an inclined elliptical vibration trajectory. Although Zhu et al. have analyzed the effects of phase shift of harmonic vibration along the X- and Y-directions on the uncut chip thickness [30], their results didn't cover the effects of an inclined elliptical vibration trajectory with fixed major and minor axes, due to the distinct definitions of phase shift and the orientation angle of the elliptical trajectory. As the following section is going to show, the ductile-to-brittle transition behavior in UEVC is significantly influenced by the orientation angle of the elliptical trajectory.

3.1. Calculation of instantaneous uncut chip thickness

In UEVC, the tool periodically engages and disengages the workpiece, which results in the variation of instantaneous uncut chip thickness (UCT) in each vibration cycle. The position where the tool starts to disengage the workpiece separates two conditions for the calculation of instantaneous UCT. When the tool position disengaging the workpiece is right on the uncut surface, the nominal DOC is termed as the characteristic DOC_m. In this study, the calculation of instantaneous UCT considers two different levels of DOC that is separated by the DOC_m. The DOC_m will be analytically defined firstly, followed by the instantaneous UCT derivation for DOC > DOC_m and DOC < DOC_m.

3.1.1. Calculation of DOC_m
Fig. 8 illustrates the definition and the calculation procedure for instantaneous UCT during one vibration cycle. The red and blue lines indicate the current and previous vibration trajectories with the arrows indicating the motion direction. The elliptical trajectory can be described in the tool coordinate system by

$$\begin{cases} x = A_x \sin\left(2\pi f_1 t + \phi_x\right) + v_c t \\ y = A_y \sin\left(2\pi f_1 t + \phi_y\right) \end{cases} \quad (5)$$

where v_c is the nominal cutting speed. A_x, A_y and ϕ_x, ϕ_y are the amplitudes and phases of the harmonic vibration along the X- and Y-directions
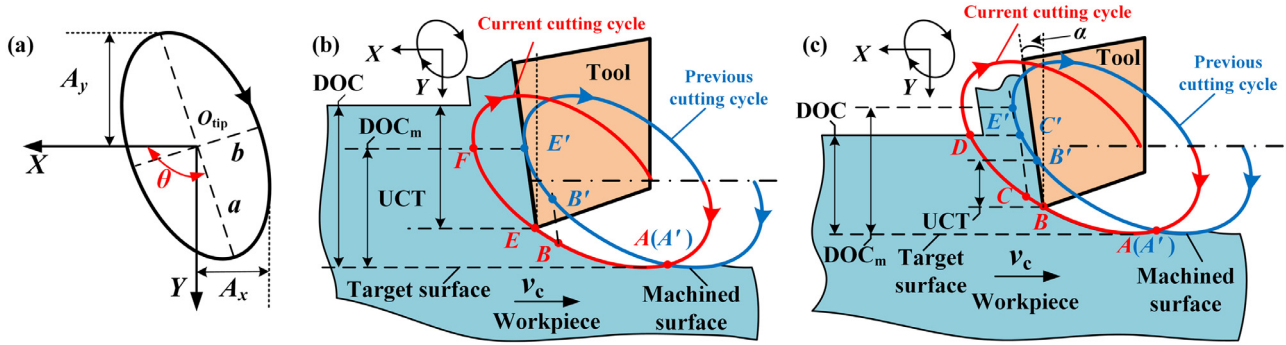
Fig. 8. (a) Definition of elliptical trajectory. Illustration of elliptical vibration cutting of brittle materials with oblique elliptical trajectories: (b) DOC > DOC$_m$; (c) DOC < DOC$_m$.

respectively, which can be calculated from the parameters of elliptical trajectory according to the following equations,

$$
\begin{cases}
A_x = \sqrt{a^2\cos^2\theta + b^2\sin^2\theta} \\
A_y = \sqrt{a^2\sin^2\theta + b^2\cos^2\theta} \\
\phi_x = \begin{cases} \arctan\left(-\dfrac{b\tan\theta}{a}\right), 0 \le \theta \le \pi/2 \\ \arctan\left(-\dfrac{b\tan\theta}{a}\right) + \pi, \pi/2 < \theta < \pi \end{cases} \\
\phi_y = \arctan\left(\dfrac{b}{a\tan\theta}\right)
\end{cases} \tag{6}
$$

where a and b are the half-length of major and minor axes of the ellipse; θ is the orientation angle of the ellipse as shown in Fig. 8(a).

In UEVC, the tool periodically contacts and separates from the workpiece. As shown in Fig. 8(b), in the previous cutting cycle, the tool starts cutting at point A' (the original position of tool), passes point B', then reaches point E', where the tool begins disengaging the workpiece. For the remaining time in the previous cutting cycle, the tool keeps disengaged from the workpiece. While in the current cutting cycle, the tool intersects with the previous cutting cycle at point A, which has the same position coordinate of point A'. Then, the tool passes points B and E, and reaches point F, whose y-coordinate is identical to that of point E'. The lines BB' and EE' are parallel to the tool rake face, while EE' is also tangent to the tool trajectory in the previous cutting cycle.

The characteristic DOC$_m$ is defined when the tool-workpiece separation point E' is right on the workpiece uncut surface. DOC$_m$ can be derived by the following equation according to the fact that EE' is a tangent line of the tool trajectory of the previous cutting cycle,

$$
\begin{cases}
\dfrac{dx}{dy}\Big|_{t_{E'}} = \dfrac{2\pi f_1 A_x \cos(2\pi f t_{E'} + \phi_x) + v_c}{2\pi f_1 A_y \cos(2\pi f t_{E'} + \phi_y)} = -\tan\alpha \\
\text{DOC}_m = A_y - y_{E'}
\end{cases} \tag{7}
$$

3.1.2. Derivation of UCT

After obtaining the characteristic DOC$_m$ through Eq. (7), the instantaneous UCT during one vibration cycle can be calculated for two different conditions where the nominal DOC is larger or smaller than the characteristic DOC$_m$.

i) When DOC > DOC$_m$ as shown in Fig. 8(b)

For arbitrary t_B satisfying $t_A \le t_B \le t_F$, the uncut chip thickness at an arbitrary point B in the current cutting cycle can be calculated by

$$
\text{UCT}(t_B) = \begin{cases} y_B - y_{B'}, t_A \le t_B \le t_E \\ \text{DOC} - (A_y - y_B), t_E < t_B \le t_F \end{cases} \tag{8}
$$

The time instance where the cutting starts can be derived by the condition that A and A' are the intersection points of two cutting cycles by

$$
\begin{cases}
x(t_A) = x(t_{A'}) \\
2\pi f_1(t_A + t_{A'}) + 2\phi_y = 3\pi \\
2\pi f_1(t_A - t_{A'}) > \pi
\end{cases} \tag{9}
$$

According to the conditions that BB' and EE' are parallel to the tool rake face, and $E'F$ is parallel to the uncut workpiece surface, $t_{B'}$, t_E and t_F in Eq. (8) can be derived through the following equations,

$$
\begin{cases}
\dfrac{x_B - x_{B'}}{y_B - y_{B'}} = -\tan\alpha \\
\dfrac{x_E - x_{E'}}{y_E - y_{E'}} = -\tan\alpha \\
t_F = t_{E'} + 1/f_1
\end{cases} \tag{10}
$$

ii) When DOC < DOC$_m$ as shown in Fig. 8(c)

For arbitrary t_B satisfying $t_A \le t_B \le t_D$, the instantaneous uncut chip thickness at an arbitrary point B can be calculated by

$$
\text{UCT}(t_B) = \begin{cases} y_B - y_{B'}, t_A \le t_B \le t_C \\ \text{DOC} - (A_y - y_B), t_C < t_B \le t_D \end{cases} \tag{11}
$$

where points C' and D are on the uncut surface in the two cutting cycles respectively. CC' is parallel to the tool rake face. According to the above conditions, the time instances at points C', D and C can be derived from the following equations,

$$
\begin{cases}
t_{C'} = \left(\pi - \arcsin\left(\dfrac{A_y - \text{DOC}}{A_y}\right) - \phi_y\right)/(2\pi f_1) \\
t_D = t_{C'} + \dfrac{1}{f_1} \\
\dfrac{x_C - x_{C'}}{y_C - y_{C'}} = -\tan\alpha
\end{cases} \tag{12}
$$

3.2. Effects of the orientation angle of elliptical trajectory on maximum uncut chip thickness

Using Eqs. (8) and (11) along with Eqs. (5) and (6), the variation of instantaneous UCT in one cutting cycle with different nominal DOCs and orientation angles of the elliptical trajectory can be calculated. The maximum UCT in one cutting cycle, which determines the critical condition, then can also be derived for various DOCs and orientation angles.

When the nominal DOC ranges from 0.3 μm to 1 μm, while the vibration trajectory is a circle ($a = b = 1$ μm) and the cutting velocity-frequency ratio is 0.1 ($v_c/f_1 = 0.1$ μm), the characteristic DOC$_m$ under such conditions is calculated to be 0.672 μm according to Eq. (7). The corresponding variation of instantaneous UCT under different DOCs can be obtained based on Eqs. (8) and (11), with results shown in Fig. 9. For a fixed DOC, the instantaneous uncut chip thickness increases first to a maximum value UCT$_m$ and then decreases to zero in one cutting cycle. For different DOCs, when the DOC exceeds the characteristic DOC$_m$, there is a sudden increase of UCT, which might induce crack-sensitive impact force in the cutting of brittle materials. In order to leverage the advantage of UEVC, the DOC$_m$ is the maximum permitted nominal cutting depth which avoids the sudden increase of uncut chip thickness. Hence, a DOC that is smaller than the DOC$_m$ is preferable in the ductile UEVC of brittle materials.
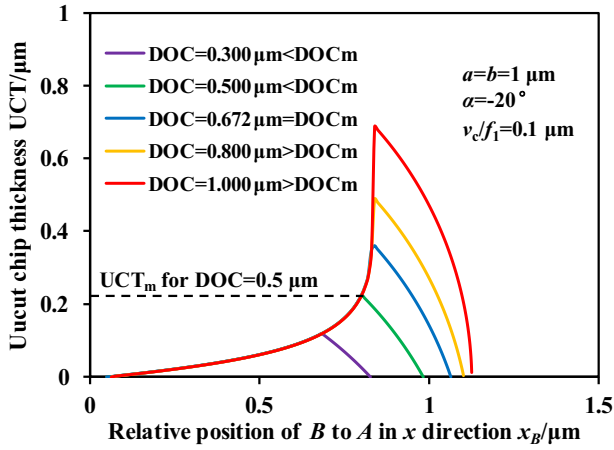
Fig. 9. Instantaneous uncut chip thickness of one cutting cycle under different DOCs.

DOC_m indicates a sudden jump of instantaneous uncut chip thickness. A higher DOC_m allows a larger nominal DOC in UEVC. In order to investigate the influence of orientation angle θ of elliptical trajectory on DOC_m, we keep the tool vibration amplitudes $a = 3$ μm and $b = =1$ μm unchanged, but only change the orientation angle θ from 0° to 180° The results are plotted in Fig. 10(a). The DOC_m varies with the increasing orientation angle θ. The valley and peak values along the DOC_m curve are around 45° and 135° of the orientation angles. These two orientation angles are also commonly seen in existing studies of UEVC due to the imperfect balance of the structural design. The influence of orientation angle of the elliptical trajectory is often not considered or evaluated for cutting brittle materials in previous studies, where a 45° [18, 31] or 0° [19, 20] was adopted by default. We find in this study, however, that an orientation angle of around 135° is optimal to obtain a larger DOC_m, thus a larger ductile-to-brittle transition depth, as shown in Fig. 10(a) (seven times larger than that of 45°). The results will be further evaluated in our experimental section.

The orientation angle of the elliptical trajectory not only significantly affects the DOC_m, but also determines the maximum value of UCT_m in one cutting cycle. The UCT_m is the critical parameter that determines the maximal allowable cutting depth for UEVC for ductile-regime cutting, which is usually set smaller than a critical value. We evaluate the variation of UCT_m with increasing DOC from zero to DOC_m when the orientation angles θ are set at 45° and 135° respectively, while keeping the vibration amplitudes $a = 3$ μm and $b = =1$ μm unchanged. The re-

sults are shown in Fig. 10(b). When the orientation angle is set at 135°, the UCT_m is always much smaller than the nominal DOC; while for the orientation angle of 45°, the UCT_m grows almost following the trend of DOC, which will set the cutting to the brittle fracture regime much faster. The orientation angle of 135° will ensure the best performance of UEVC in terms of increasing the nominal DOC in ductile-regime cutting of brittle materials. Moreover, the slope in the DOC_m curve at 135° (as shown in Fig. 10(a)) is zero, which will help to provide a stable ductile cutting condition even with a slight angle variation of the elliptical trajectory.

The orientation angle of elliptical trajectory might also affect the service life of cutting tool, which is another important performance indicator in the ultrasonic surface texturing process. The best elliptical trajectory with the orientation angle of 135° is expected to be beneficial to the tool service life due to its superiority in the reduction of uncut chip thickness. Further evaluation of the role of elliptical trajectory in the tool tip degradation is worthy of further study in the future.

4. Grooving tests and surface texturing on silicon

In order to verify our proposed theory and to investigate the effects of ductile-regime texturing of brittle materials using the proposed combined vibration tool, two sets of experiments were designed and conducted on a customized machining platform (see Appendix A). The first set of grooving experiments were designed to verify the theoretical analysis, particularly to identify the effect of elliptical orientation angles on the critical ductile-to-brittle depth. The second set of experiments utilized the combined high-frequency and low-frequency vibration to achieve modulated UEVC of micro-structured silicon with crack-free surfaces. The detailed experimental conditions are summarized in Table 1.

4.1. Grooving experiments on single crystal silicon

In order to verify the theoretical analysis results of the develop UCT model, grooving experiments were conducted on a tilted silicon workpiece with a tilt angle of 2 μm/mm. In the grooving experiments, the developed tool vibrated at 2 kHz to generate inclined elliptical trajectories with orientation angles of 135° and 45° respectively. The 135° angle corresponds to the optimal cutting condition based on our model, which also coincides with the resonant vibration trajectories generated by the developed tool. The 45° is the comparison set which corresponds to the least favorable condition in UEVC (the lowest point in Fig. 10(a)). The nominal cutting speed was set to 12 mm/min to match the cutting velocity-frequency ratio ($v_c/f_1 = 0.1$ μm). Moreover, the conventional cutting without tool vibration was also conducted at a nominal cutting speed of 12 mm/min.
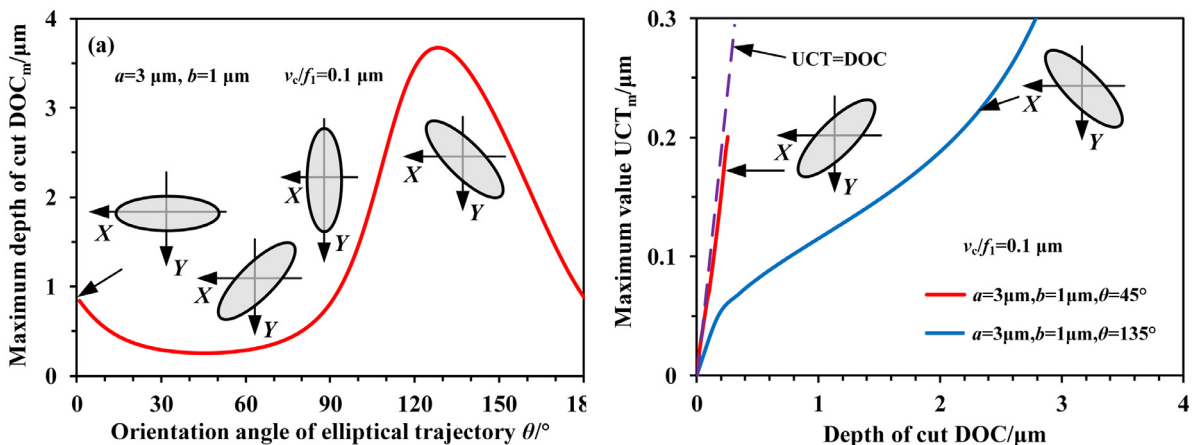

Fig. 10. (a) Effect of the orientation angle of elliptical trajectory on DOC_m; (b) variation of maximum uncut chip thickness with an increasing DOC.

Table 1

Experimental conditions.

Machining conditions			
Silicon properties	Crystal plane	(100)	
	Crystal orientation	[110] along cutting direction	
Diamond tool parameters	Nose radius	470 μm	
	Rake angle	−20°	
	Clearance angle	10°	
Set 1	Cutting parameters	Nominal cutting speed	12 mm/min
		Workpiece tilt angle	2 μm/mm
	Vibration parameters	Trajectory	$a = 3$ μm, $b = 1$ μm, $\theta = 45°$ or $135°$, 2000 Hz; and conventional cutting without tool vibration
Set 2	Cutting parameters	Nominal cutting speed	120 mm/min
		Cross feed	100 μm
	Vibration parameters	Resonant vibration	20 kHz, $U_{1L,0-p} = U_{1R,0-p} = 1.5$ V, $\alpha_1 = 180°$
		Non-resonant vibration	100 Hz, $U_{2L,0-p} = U_{2R,0-p} = 7.5$ V, $\alpha_2 = 90°$
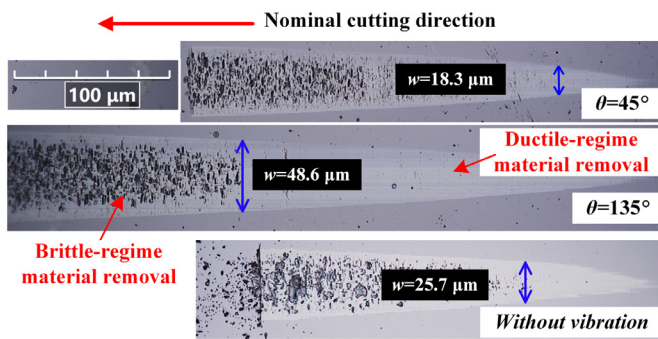
Fig. 11. Experimental results on the effects of orientation angle of the elliptical trajectory on the ductile cutting depth ($v_c/f_1 = 100$ nm).

Fig. 12. Tool motion trajectory for surface texturing of silicon with combined resonant and non-resonant vibrations.

The cutting results are compared in Fig. 11 with the optical images of the grooved silicon. As shown in Fig. 11, the width w of the grooved surface increases from right to left due to the increase of DOC. The surface quality of grooved silicon deteriorates sharply when the cutting width w exceeds a critical value, which indicates the transition of material removal state from ductile-regime to brittle-regime. According to the relationship between cutting width w and DOC shown in Fig. A1(b), the critical DOCs of ductile-to-brittle transition for the conventional cutting without tool vibration is calculated to be 176 nm, while the critical DOCs for the 45° and 135° cases are 89 nm and 628 nm respectively. Even though both results were machined by elliptical vibration cutting, it has been demonstrated here that the orientation angle of the elliptical trajectory is critical to determine the performance of UEVC in ductile-regime cutting of brittle materials. As predicted by our model as shown in Fig. 10, the orientation angle of 135° outperforms that of 45° by increasing the critical DOC up to seven times. Moreover, the elliptical vibration cutting with an orientation angle of 45° even reduces critical DOC over conventional cutting without tool vibration.

4.2. Surface texturing on single crystal silicon with modulated UEVC

We investigated the efficacy of proposed modulated UEVC in texturing micro-structured surface on brittle materials in this section. The micro-dimples arrays were generated using combined resonant and non-resonant vibrations (modulated UEVC) as well as just the conventional diamond cutting. The results were then compared to demonstrate the process capability.

The combined resonant and non-resonant vibrations were simultaneously generated by the developed tool. The ultrasonic elliptical vibration was excited at the tool resonant frequency of 20 kHz, where the
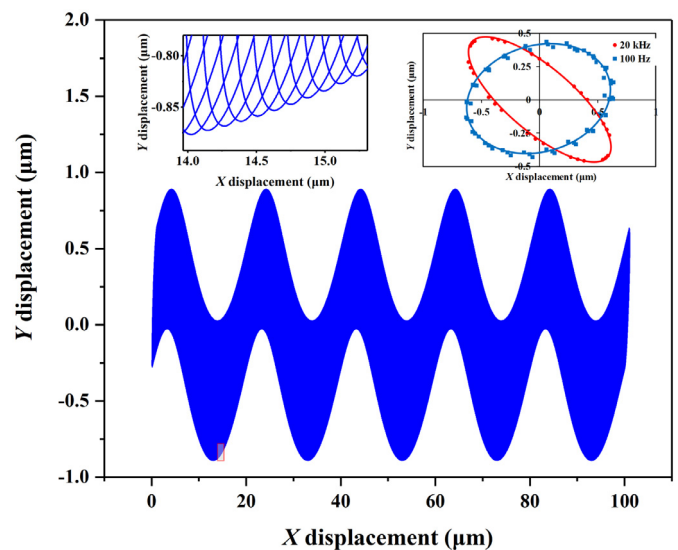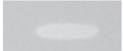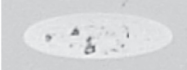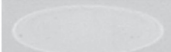
vibration amplitudes were recorded at 0.6 μm and 0.5 μm in cutting and DOC direction respectively. The elliptical trajectory orientation angle was 135° corresponding to the optimal cutting condition. The non-resonant modulated motion was generated at 100 Hz, with vibration amplitudes of 0.6 μm and 0.4 μm and an orientation angle of 20°. The combined tool trajectories were measured a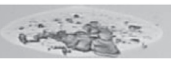s shown in Fig. 12. The ultrasonic vibration was used to enhance the ductile-regime cutting of brittle materials, while the low-frequency modulation motion was utilized to shift the vibration center for creating micro-structures (dimples).

The dimple arrays were generated with and without modulated UEVC. The resonant and non-vibration were kept unchanged, while the nominal DOC was increased from 100 nm to 1200 nm with a 100 nm increment. For each cutting line, one hundred consecutive dimples were generated. The cross-feed was set to 100 μm, and the DOC was set to increase with a rate of 100 nm per cross-feed motion. The experiments were repeated by disabling the ultrasonic vibration but only with the 100 Hz modulation motion. The surface morphologies of both samples were observed and compared to identify the critical cutting conditions to achieve ductile-regime texturing of silicon surfaces.

Fig. 13 demonstrates the dimple arrays machined with modulated UEVC for the nominal DOCs from 300 nm to 500 nm (from the right to the left). The ratio of nominal cutting velocity over the modulation frequency (v_c/f_2) is 20 μm, which determines the dimple interval along the

Table 2
Morphology of machined dimples with and without UEVC (width w/μm, depth DOC/nm).

Depth	0-100 nm	100-200 nm	200-300 nm	300-400 nm
With UEVC	w= 18.9, DOC=95	w=25.6, DOC= 175	w = 31, DOC =257	w =35.9, DOC =343
Without UEVC	w =13.5, DOC= 48	w =23.6, DOC= 148	w =31.7, DOC= 268	w =37.8, DOC = 380

Depth	400-500 nm	500-600 nm	600-700 nm	700-800 nm
With UEVC	w =40.5, DOC= 437	w =44.5, DOC =529	w = 48.6, DOC=629	w =53.3, DOC = 758
Without UEVC	w=40.5, DOC = 437	w =45.9, DOC = 561	w =50.0, DOC=665	w =52.7, DOC =739

Depth	800-900 nm	900-1000 nm	1000-1100 nm	1100-1200 nm
With UEVC	w =57, DOC =878	w =59.4, DOC =941	w = 62.8, DOC =1051	w =64.8, DOC =1120
Without UEVC	w =56.7, DOC =857	w =59.5, DOC =941	w =63, DOC =1074	w =66.2, DOC =1167
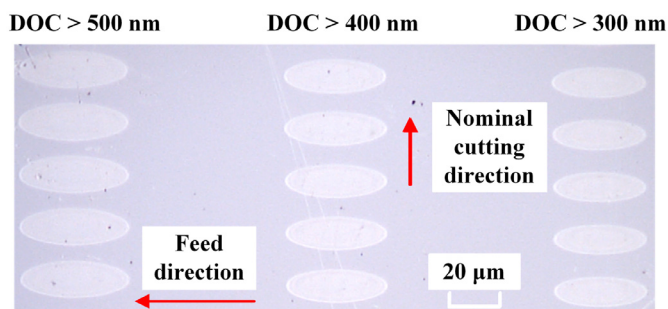
Fig. 13. Textured surface of micro dimple arrays with modulated UEVC.

cutting direction. The dimple width also increases with the increment of DOC due to the tool nose radius. According to the developed model in Section 3, the calculated DOC_m for the elliptical trajectory used in this experiment is 710 nm, while the maximal UCT_m is 160 nm. For a nominal DOC smaller than DOC_m (710 nm), the UCT will be kept much smaller than the nominal DOC, thus to leverage the advantage of UEVC for much enhanced critical cutting depth. As shown by the machined results in Fig. 13, crack-free dimple arrays have been successfully fabricated based on our proposed modulated UEVC.

The surface morphologies of micro dimples generated with and without modulated UEVC are also compared to verify the much-extended ductile regime for surface texturing. With the additional ultrasonic vibration, it is difficult to maintain the exact same DOC for cutting with and without vibrations. Even if the very accurate vibration amplitude and nominal DOC is applied, the material might respond differently. So the actual measured cutting width w and DOC are obtained from the surface morphologies. The results are summarized in Table 2.

Without the ultrasonic elliptical vibration, severe and obvious cracks can be observed on the micro dimple surface just when the DOC is above 200 nm. In comparison, when the modulated UEVC is employed, crack-free dimple surface has been successfully created up to a nominal DOC of 700 nm, which also agrees with the predicted DOC_m of 710 nm by Eq. (7). When the DOC exceeds DOC_m, the impact cutting force induced by the sudden increase of instantaneous UCT is prone to induce brittle fracture during machining. What is further observed is that even when the DOC exceeds DOC_m, only a slight marring can be observed on micro dimple surfaces up to the DOC of 1 μm. While for surface texturing without UEVC, severe cracks appear right after the critical cutting depth. This can be attributed to the fact that the maximal UCT during a cutting cycle is not at the lowest cutting point (or away from the machined surface), so only very few induced cracks are propagated to the machined surface. In practice, however, the DOC_m is still recommended to be the applicable maximum DOC to ensure a ductile-regime textur-

ing during the whole cutting cycle. The above experimental results in Table 2 demonstrate that the ductile cutting depth of micro dimples with modulated UEVC can be dramatically improved over that without ultrasonic elliptical vibration. This conclusion also agrees with the predictive results of the developed model as shown in Fig. 10(b).

5. Conclusions

This study is devoted to adopting ultrasonic elliptical vibration cutting (UEVC) to texture micro-structured surfaces on brittle materials in the ductile regime. A modulated UEVC process is proposed with a newly developed 2-D vibration cutting tool, which can provide combined resonant and non-resonant vibrations in a single structure. The ultrasonic elliptical vibration at 20 kHz is used to enhance the ductile-to-brittle transition depth, while the simultaneously generated non-resonant modulation motion (up to 2 kHz) is used to adjust the tool center to generate surface structures dynamically. Based on the theoretical analysis and experimental results, the following conclusions can be drawn.

(1) The proposed new tool has a compact structure with its first two resonant frequencies in the ultrasonic range. So, the coupled resonant vibration is used to generate elliptical vibration trajectory, while the non-resonant motion can be superimposed utilizing the flat frequency response in the low-frequency range.

(2) A more general UCT model in elliptical vibration cutting of brittle materials is developed by considering the orientation angle of elliptical trajectory on ductile cutting performance. The developed model suggests that an orientation angle of 135° is the optimal angle to achieve the largest nominal DOC for ductile regime cutting, which is also verified by our experimental results. The elliptical vibration cutting with an orientation angle of 45° even reduces critical DOC over conventional cutting without vibration.

(3) Micro dimple arrays, with a maximum depth of 700 nm in ductile-regime and an extended DOC up to 1 μm with minimal surface damage, have been successfully generated on silicon surfaces with modulated UEVC. In comparison, the damage-less maximal depth of less than 200 nm is achieved without UEVC. Moreover, compared with the vibration amplitude control method, the modulated UEVC avoids the possible violation of ductile cutting condition due to the unchanged amplitudes, enabling a more robust design of elliptical vibration trajectories.

Declaration of Competing Interest

None.

CRediT authorship contribution statement

Jianjian Wang: Methodology, Investigation, Writing - original draft. **Wei-Hsin Liao:** Supervision, Funding acquisition. **Ping Guo:** Conceptualization, Methodology, Writing - review & editing, Supervision, Funding acquisition.

Appendix A. Machining platform description

The customized machining platform is shown in Fig. A1(a). It consists of a three-axis nano-positioning stage (ACT130, *Aerotech, Pittsburgh, USA*), and a direct-drive linear actuator (ACT165DL, *Aerotech, Pittsburgh, USA*). The three-axis nano-positioning stage is used to generate feed motion of silicon workpiece, while the direct-drive linear actuator is used to generate the nominal cutting motion. The silicon wafer with a dimension of 10 mm × 10 mm × 0.67 mm is mounted on a two-degree-of-freedom tilt stage, which is used for level adjustment of the workpiece with the help of a capacitive displacement sensor. The developed tool is mounted on the direct-drive linear actuator. A commercial single crystal diamond insert with a nose radius R of 470 μm, a rake angle of −20° and a clearance angle of 10° is mounted on the end effector of the developed tool. A single-lens reflex camera is used for tool setting. The machined surface structures were observed and the cutting widths were measured with a digital microscope (RH-2000, *Hirox, Tokyo, Japan*). The effect of DOC on the cutting width is calculated and shown in Fig. A1(b), which can be used to obtain the actual DOC from the cutting width w ([16]).
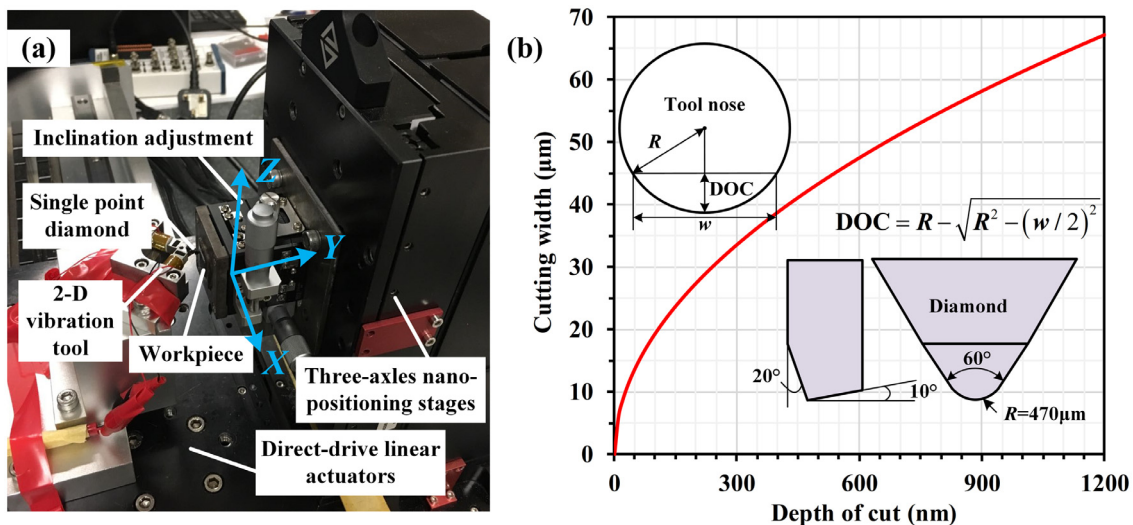

Fig. A1. (a) Experiment setup of surface texturing; (b) cutting depth calculation.

References

[1] Sun Z, To S, Yu KM. One-step generation of hybrid micro-optics with high-frequency diffractive structures on infrared materials by ultra-precision side milling. Opt Express 2018;26:28161–77.

[2] Liu S, Mulligan JA, Adie SG. Volumetric optical coherence microscopy with a high space-bandwidth-time product enabled by hybrid adaptive optics. Biomed Opt Express 2018;9:3137–52.

[3] Bulla B, Klocke F, Dambon O. Analysis on ductile mode processing of binderless, nano crystalline tungsten carbide through ultraprecision diamond turning. J Mater Process Technol 2012;212:1022–9.

[4] Antwi EK, Liu K, Wang H. A review on ductile mode cutting of brittle materials. Front Mech Eng 2018;13:251–63.

[5] Yue X, Xu M, Du W, Chu C. Effect of cutting edge radius on surface roughness in diamond tool turning of transparent MgAl$_2$O4 spinel ceramic. Opt Mater 2017;71:129–35.

[6] Leung TP, Lee WB, Lu XM. Diamond turning of silicon substrates in ductile-regime. J Mater Process Technol 1998;73:42–8.

[7] Mukaida M, Yan J. Ductile machining of single-crystal silicon for microlens arrays by ultraprecision diamond turning using a slow tool servo. Int J Mach Tool Manuf 2017;115:2–14.

[8] Brinksmeier E, Gläbe R, Schönemann L. Review on diamond-machining processes for the generation of functional surface structures. CIRP J Manuf Sci Tech 2012;5:1–7.

[9] Zhu Z, To S, Xiao G, Ehmann KF, Zhang G. Rotary spatial vibration-assisted diamond cutting of brittle materials. Precis Eng 2016;44:211–19.

[10] Liu H, Xie W, Sun Y, Zhu X, Wang M. Investigations on brittle-ductile cutting transition and crack formation in diamond cutting of mono-crystalline silicon. Int J Adv Manuf Technol 2018;95:317–26.

[11] Zhang J, Cui T, Ge C, Sui Y, Yang H. Review of micro/nano machining by utilizing elliptical vibration cutting. Int J Mach Tool Manuf 2016;106:109–26.

[12] Suzuki N, Masuda S, Haritani M, Shamoto E. Ultraprecision micromachining of brittle materials by applying ultrasonic elliptical vibration cutting. In: Proceedings of the 2004 International symposium on MHS; 2004. p. 133–8.

[13] Zhang J, Suzuki N, Wang Y, Shamoto E. Fundamental investigation of ultra-precision ductile machining of tungsten carbide by applying elliptical vibration cutting with single crystal diamond. J Mater Process Technol 2014;214:2644–59.

[14] Geng D, Liu Y, Shao Z, Lu Z, Cai J, Li X, et al. Delamination formation, evaluation and suppression during drilling of composite laminates: a review. Compos Struct 2019;216:168–86.

[15] Nath C, Rahman M, Neo K S. Modeling of the effect of machining parameters on maximum thickness of cut in ultrasonic elliptical vibration cutting. J Manuf Sci Eng 2011;133:11007.

[16] Huang W, Yu D, Zhang X, Zhang M, Chen D. Ductile-regime machining model for ultrasonic elliptical vibration cutting of brittle materials. J Manuf Process 2018;36:68–76.

[17] Zhou X, Zuo C, Liu Q, Lin J. Surface generation of freeform surfaces in diamond turning by applying double-frequency elliptical vibration cutting. Int J Mach Tool Manuf 2016;104:45–57.

[18] Kurniawan R, Ko TJ, Ping LC, Kumaran ST, Kiswanto G, Guo P, et al. Development of a two-frequency, elliptical-vibration texturing device for surface texturing. J Mech. Sci Technol 2017;31:3465–73.

[19] Kurniawan R, Kiswanto G, Ko TJ. Surface roughness of two-frequency elliptical vibration texturing (TFEVT) method for micro-dimple pattern process. Int J Mach Tool Manuf 2017;116:77–95.

[20] Suzuki N, Yokoi H, Shamoto E. Micro/nano sculpturing of hardened steel by controlling vibration amplitude in elliptical vibration cutting. Precis Eng 2011;35:44–50.

[21] Zhang J. Micro/Nano machining of steel and tungsten carbide utilizing elliptical vibration cutting technology Ph.D. thesis; 2014.

[22] Zhang J, Zhang J, Cui T, Hao Z, Zahrani A A. Sculpturing of single crystal silicon microstructures by elliptical vibration cutting. J Manuf Process 2017;29:389–98.

[23] Wang J, Yang Y, Guo P. Effects of vibration trajectory on ductile-to-brittle transition in vibration cutting of single crystal silicon using a non-resonant tool. Procedia CIRP 2018;71:289–92.

[24] Zhou X, Zuo C, Liu Q, Wang R, Lin J. Development of a double-frequency elliptical vibration cutting apparatus for freeform surface diamond machining. Int J Adv Manuf Technol 2016;87:2099–111.

[25] Yuan Y, Zhang D, Jing X, Zhu H, Zhu W, Cao J, et al. Fabrication of hierarchical freeform surfaces by 2D compliant vibration-assisted cutting. Int J Mech Sci 2019;152:454–64.

[26] Yang Y, Gao S, Chen K, Pan Y, Guo P. Vibration analysis and development of an ultrasonic elliptical vibration tool based on a portal frame structure. Precis Eng 2017;50:421–32.

[27] Chen K, Si C, Guo P. Design of a high bandwidth nonresonant tertiary motion generator for elliptical vibration texturing. J Micro Nano-Manuf 2017;5:11008.

[28] Dai J, Su H, Yu T, Hu H, Zhou W, Ding W. Experimental investigation on materials removal mechanism during grinding silicon carbide ceramics with single diamond grain. Precis Eng 2018;51:271–9.

[29] Wang W, Yao P, Wang J, Huang C, Zhu H, Zou B, et al. Crack-free ductile mode grinding of fused silica under controllable dry grinding conditions. Int J Mach Tool Manuf 2016;109:126–36.

[30] Zhu W, He Y, Ehmann KF, Zhu Z, Ju B. Modeling of the effects of phase shift on cutting performance in elliptical vibration cutting. Int J Adv Manuf Technol 2017;92:3103–15.

[31] Zhu WL, He Y, Ehmann KF, Egea A, Wang X. Theoretical and experimental investigation on inclined ultrasonic elliptical vibration cutting of alumina ceramics. J Manuf Sci Eng 2016;138:121011.